Oriented imaging of 3D subcellular structures in bacterial cells using optical tweezers

G. Carmon,[1,2] I. Fishov,[3] and M. Feingold[1,2,*]

[1]*Department of Physics, Ben-Gurion University of the Negev, Beer Sheva 84105, Israel*

[2]*The Ilse Katz Center for Nanotechnology, Ben-Gurion University of the Negev, Beer Sheva 84105, Israel*

[3]*Department of Life Sciences, Ben-Gurion University of the Negev, Beer Sheva 84105, Israel*

**Corresponding author: mario@bgu.ac.il*

Received September 15, 2011; revised December 12, 2011; accepted December 12, 2011; posted December 13, 2011 (Doc. ID 154104); published February 1, 2012

Using oscillating optical tweezers, we show that controlled alignment of rod-shaped bacterial cells allows imaging fluorescently labeled three-dimensional (3D) subcellular structures from different, optimized viewpoints. To illustrate our method, we analyze the Z ring of *E. coli*. We obtain that the radial width of the Z ring in unconstricted cells is about 120 nm. This result suggests that the Z ring consists of an extremely sparse network of FtsZ filaments. © 2012 Optical Society of America

OCIS codes: 180.6900, 110.2960.

Optical microscopy is one of the main tools of cell biology. It allows monitoring intracellular processes in both space and time. To resolve the three-dimensional (3D) structure of individual cells, confocal microscopy [1], optical coherence tomography [2], and deconvolution methods [3] have been developed. These techniques rely on scanning the object along the optical axis to image the different z slices. Such slice images are used subsequently to reconstruct a 3D representation of the cell. Since optical resolution along the optical axis, z, is lower than that in the (x, y) plane, z slicing might not be the best approach to obtain the 3D structure of thin cells, e.g., bacteria. Alternatively, one may view cells from different angles relative to the optical axis and use the resulting projections to obtain information about their 3D organization. This approach is analogous to that of cryo-electron tomography [4]. Recently, we have shown that controlled alignment of rod-shaped cells can be achieved using oscillating optical tweezers [5,6]. In this letter, we employ the cell alignment technique to image and characterize protein assemblies in individual *E. coli* cells. In particular, the study of the Z ring illustrates the advantages of aligned cell imaging.

In bacteria, the cytoskeletal tubulin homolog, FtsZ, is the central element of the cell division machinery [7]. In *E. coli*, FtsZ forms a ring in the constriction plane and subsequently recruits a series of ~13 additional proteins to this so-called "Z ring." However, we still do not understand the spatial organization of the Z ring. On the one hand, cryo-electron tomography experiments on *C. crescentus* [8] showed that the Z ring consists of a few FtsZ filaments that, on average, are 120 nm long and are located at about 16 nm below the cytoplasmic membrane (CM). On the other hand, photoactivated localization microscopy (PALM) imaging of the Z ring in *E. coli* [9] found significantly higher density of FtsZ than that of Ref. [8]. In particular, their results indicate that the Z ring is multilayered in the radial direction (inward from the CM). Although the apparent disagreement between the Z ring structures observed in cryo-electron tomography experiments and in PALM imaging could be attributable to the differences between the corresponding bacteria, namely, between *C. crescentus* and *E. coli*, it highlights the need of additional quantitative information on the radial width of the Z ring. Here we use a technique that combines oscillating optical tweezers with image analysis to measure the radial width of the Z ring in unconstricted *E. coli* cells. Trapped cells can be switched between horizontal alignment, with the long axis in the plane of view, and vertical alignment [5,6]. For vertically oriented cells the Z ring image appears as a symmetrical circular structure that is significantly easier to analyze than the usual image obtained in the horizontal orientation. The main advantage of our approach lies in the ability to image a particular cell in both horizontal and vertical orientations within several seconds. While the former allows establishing its stage along the cell cycle and whether there are other FtsZ structures on the CM aside from the Z ring, the latter provides an optimal viewpoint on the Z ring.

Imaging was performed on an inverted microscope (IX70, Olympus) with a CoolSNAP ES^2 camera (Photometrics). Exposure time was 0.5 s. The pixel size corresponds to a length of 41 nm. A laser beam (SDL, $\lambda = 830$ nm) was focused through the 100× objective (UPLFLN 100XO2PH, 1.3 NA, oil immersion) to give an

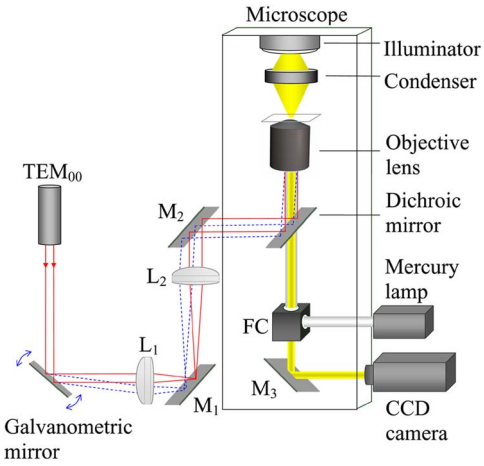

Fig. 1. (Color online) The optical system: M1, M2, and M3–mirrors, L1, L2–telescope lenses, FC–filter cube. The laser beam is shown for the case when the galvanometric mirror is at 45° (solid red line) and for a smaller angle (dashed blue line).

optical trap (Fig. 1). Since the trapping force is larger in the (x, y) plane than along the optical axis, the optical trap will align elongated objects with their long axis in the z direction (vertical view). Therefore, optical tweezers can be used to view rod-shaped *E. coli* cells along their long axis (Fig. 2). Our optical system also allows complementing the vertical image of a cell with a corresponding horizontal image. This is achieved by horizontally oscillating the position of the trap at frequencies of ~100 Hz and amplitudes slightly larger than the cell length. In this configuration, the cell experiences an effectively linear trap and therefore aligns horizontally along the direction of the oscillation. The trap oscillation is induced by means of a galvanometric mirror (Fig. 1). In both the horizontal and the vertical orientations we can image the cell in both phase contrast and fluorescence (Fig. 2). The switching time between the different imaging modes (few seconds) is shorter than the time scale of Z ring structural dynamics [10]. Finally, an adjustable telescope system located along the optical path of the laser beam allows raising and lowering the trapped cell relative to the viewing plane. This option enables us to focus on the Z ring.

For our study, we used *E. coli* strain EC488 [11]. It contains a chromosomal copy of *ftsZ-gfp* under control of a modified *trc* promoter. The expression of FtsZ-GFP was induced by either 40 μM or 500 μM isopropyl-b-D-thiogalactopyranoside (IPTG). We refer to the former case as low induction level (LIL) and to the latter as high induction level (HIL). While in LIL experiments EC488 were found to display normal growth and division behavior [12,13], in HIL experiments we observe a slowdown in the rate of growth. However, the Z-ring structure appears to be the same at both high and low inductions. Cells were grown at 37° in Luria broth until optical density ~0.2 in the exponential regime. The CM was imaged using 1 μM of the FM4-64 fluorescent stain (molecular probes).

We studied live *E. coli* cells that expressed FtsZ-GFP and had their CM stained with FM4-64. We used the horizontal orientation to select cells that (1) had no constriction, (2) displayed a clear Z ring, and (3) showed no FtsZ structures in addition to the Z ring, e.g., helices [12]. From the images of the corresponding vertically aligned cells we computed average radial profiles for both the FtsZ-GFP and FM4-64 distributions [Fig. 3(a)]. First, we determined the center of the ring with subpixel precision, finding the

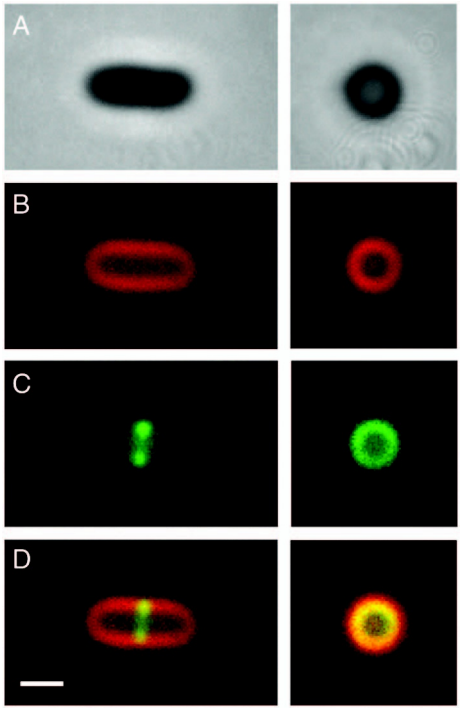

Fig. 2. A trapped unconstricted *E. coli* cell from a HIL experiment. All images are on the same scale. Bar = 1 μm. Left: horizontal orientation; Right: vertical orientation. (A) Phase contrast image, (B) FM4-64 image of the CM (red), (C) GFP image of the Z-ring (green), (D) overlay of (B) and (C). The weak red halo around the yellow ring indicates that the CM is farther from the cell axis than the Z ring.

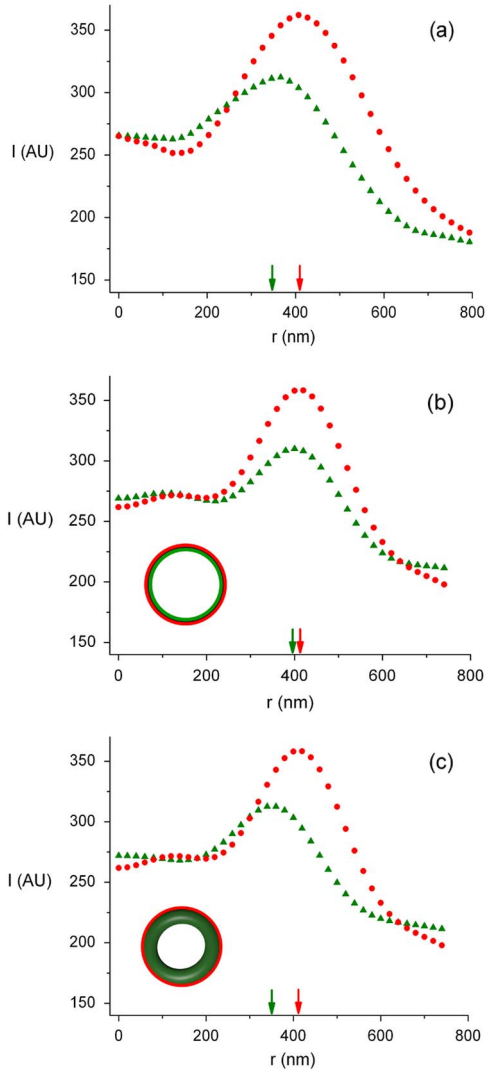

Fig. 3. (Color online) Average radial profiles. (a) for the cell of Fig. 2: the profile of the CM (red circles) and the profile of the Z-ring (green triangles), $r_{FM} = 411 \pm 3$ nm (right arrow), $r_{GFP} = 356 \pm 5$ nm (left arrow), and $\Delta r = 54 \pm 6$ nm (r_{GFP} denotes the position of the FtsZ-GFP $I(r)$ peak). (b) Same as in (a) but for a model *E. coli* cell with a cylindrical surface Z ring (see text) (inset illustrates the corresponding midcell section). The radius of the model cell is set to 430 nm such that r_{FM} is the same as in (a). Moreover, $r_{Z\text{-ring}} = 389$ nm and $\Delta r = 21$ nm. (c) Same as in (b) but for a toroidal Z ring (see text). Here, $r_{Z\text{-ring}} = 350$ nm and $\Delta r = 61$ nm.

best fitting circle to the maximal intensity contour. Next, we measured the radial intensity profile along rays that start at the center of the ring. The fluorescence intensity was obtained at 20 nm intervals along a ray using linear interpolation. The interpolation was done between the intensity values in the three nearest neighboring pixels [14,15]. Radial profiles were measured for 360 rays at equal angular intervals around the ring. Averaging these profiles leads to a smooth function, the average radial profile, $I(r)$ [Fig. 3(a)].

We have analyzed seven cells that satisfy the three requirements spelled out above. In addition, the cells were required to display in both the FM4-64 and FtsZ-GFP vertical images rings with sufficient contrast and circular symmetry. Cells with good enough contrast levels could be found only in HIL experiments. However, cells from LIL experiments with the best contrast levels available gave results similar to those of the high induction ones only with a larger spread of values and larger errors. For the seven analyzed cells we found that the peak of the FM4-64 $I(r)$ is ~60 nm farther from the cell center than the one of FtsZ-GFP. Specifically, we found that the difference in r between the peaks, Δr, was 54 ± 11 nm, 58 ± 11 nm, 55 ± 11 nm, 62 ± 11 nm, 59 ± 11 nm, 71 ± 11 nm, and 58 ± 11 nm, while the position of the FM4-64 peak itself, r_{FM}, varied from 410 nm to 535 nm. Since the outermost layer of the Z ring is attached to the CM [7], the maximal FtsZ-GFP $I(r)$ corresponds to the center of a radially extended FtsZ-GFP distribution. Accordingly, we propose that Δr is approximately equal to half the radial width of the Z ring, D.

The errors in the measured values of Δr include experimental errors of three types: (1) the variability among the nonaveraged radial profiles, $I(r, \theta)$, (2) the focusing error, and (3) errors attributable to fluctuations of the trapped cell. The average error of Δr owing to profile variability was 7 nm. To calibrate the focusing error, we used cells that were vertically immobilized in agar. Scanning the focus within a few micrometer range around the apparent focal plane allowed estimating the corresponding average error in Δr at 5 nm. Moreover, the effect of trapped cell fluctuations on the position of the $I(r)$ peak was tested by varying the strength of the trap. We find that changing the laser beam power (at the exit from the objective) between 18 mW and 61 mW (working power was 37 mW) results in fluctuations of the Δr with a standard deviation of 7 nm. We have also verified the possibility of experimental artifact attributable to the effect of chromatic aberrations. Since the emission spectra of GFP and CM bound FM4-64 are centered at different wavelengths, 507 nm and 615 nm, respectively, there could be a difference in magnification between the corresponding images. To examine the dependence of magnification on wavelength, we imaged pairs of immobilized fluorescein-coated microbeads using sequentially the GFP and FM4-64 filter sets. We found that distances between beads were the same in the two wavelength ranges within the accuracy of the position-finding algorithm (<10 nm).

Assuming no experimental artifact in measuring Δr, we considered the option that the FtsZ-GFP $I(r)$ is biased inward by the unassembled fraction of FtsZ dispersed throughout the cytoplasm (70% of the total FtsZ in the cell [10]). To verify this scenario, we simulated the behavior of $I(r)$ for the corresponding FtsZ-GFP and FM4-64 configurations. We used a theoretical 3D point spread function (3D PSF) model appropriately adjusted for the large NA objective [16]. It was found to be in good agreement with the measured PSF in the focal plane. To mimic the FtsZ distribution observed by Zhuo *et al.* [8], we considered a cell model where the Z ring is represented by a cylindrical surface parallel to the CM at 10 nm inward, centered at midcell, and extending 100 nm along the cell axis. In addition, 70% of the total FtsZ-GFP in the cell is homogenously distributed throughout the cytoplasm. Numerically convoluting this cell model with the 3D PSF leads to $\Delta r = 21$ nm, much smaller than the measured Δr [Fig. 3(b)]. To reproduce the values of Δr measured in our experiments, a second cell model was simulated that had the same distribution of FtsZ in the cytoplasm as before and a toroidal Z ring located at midcell [Fig. 3(c)]. The minor and major radii of the torus were $r_1 = 60$ nm and $r_2 = 370$ nm, respectively, such that it extended up to the CM. In fact, the toroidal Z-ring model was proposed by Fu *et al.* to account for their results [9]. For this case, we obtained $\Delta r = 61$ nm, in good agreement with experiment. Moreover, while Δr was almost independent of r_2 and of flattening the torus toward midcell, it changed rapidly with r_1.

In conclusion, we have used optical tweezers and subpixel image analysis to estimate D, the radial width of the Z ring in *E. coli*. We found that $D \sim 2\Delta r \sim 120$ nm. This value is consistent with the observations of Fu *et al.* [9]. Because the amount of FtsZ in the Z ring is limited [10], our findings suggest that the Z ring consists of a sparse, multilayered network of FtsZ filaments.

We thank Y. Garini and Y. Meir for useful discussions. This research was supported in part by the Israel Academy of Science and Humanities (Grant No. 1544/08).

References

1. R. H. Webb, Rep. Prog. Phys. **59**, 427 (1996).
2. D. Huang, E. Swanson, C. P. Lin, J. S. Schuman, W. G. Stinson, W. Chang, M. R. Hee, T. Flotte, K. Gregory, C. A. Puliafito, and J. G. Fujimoto, Science **254**, 1178 (1991).
3. J. B. Sibarita, Adv. Biochem. Eng. Biotechnol. **95**, 201 (2005).
4. K. Grunewald, O. Medalia, A. Gross, A. C. Steven, and W. Baumeister, Biophys. Chem. **100**, 577 (2003).
5. G. Carmon and M. Feingold, Opt. Lett. **36**, 40 (2011).
6. G. Carmon and M. Feingold, J. Nanophoton. **5**, 051803 (2011).
7. D. W. Adams and J. Errington, Nat. Rev. Microbiol. **7**, 642 (2009).
8. L. Zhuo, M. J. Trimble, Y. V. Brun, and G. J. Jensen, EMBO J. **26**, 4694 (2007).
9. G. Fu, T. Huang, J. Buss, C. Coltharp, Z. Hensel, and J. Xiao, Plos ONE **5**, e12680 (2010).
10. J. Stricker, P. Maddox, E. D. Salmon, and H. P. Erickson, Proc. Natl. Acad. Sci. USA **99**, 3171 (2002).
11. D. S. Weiss, J. Chen, J. Ghigo, D. Boyd, and J. Beckwith, J. Bacteriol. **181**, 508 (1999).
12. S. Thanedar and W. Margolin, Curr. Biol. **14**, 1167 (2004).
13. R. Tsukanov, G. Reshes, G. Carmon, E. Fischer-Friedrich, N. S. Gov, I. Fishov, and M. Feingold, Phys. Biol. **8**, 066003 (2011).
14. G. Reshes, S. Vanounou, I. Fishov, and M. Feingold, Biophys. J. **94**, 251 (2008).
15. E. Itan, G. Carmon, A. Rabinovitch, I. Fishov, and M. Feingold, Phys. Rev. E **77**, 061902 (2008).
16. M. Gu, *Advanced Optical Imaging Theory* (Springer-Verlag, 2000).